*Anal. Bioanal. Electrochem., Vol. 11, No. 1, 2019, 38-48*

***Analytical &***
***Bioanalytical***
***Electrochemistry***

2019 by CEE
www.abechem.com

*Full Paper*

# Effect of Sodium Phosphate Concentration on Corrosion Behavior of the Coatings Produced by Plasma Electrolytic Oxidation (PEO) on AZ31B Mg Alloy in Body Simulative Fluid

**Razieh Chaharmahali, Mozhgan Shadabi, Kazem Babaei, Seyed Omid Gashti and Arash Fattah-alhosseini***

*Department of Materials Engineering, Bu-Ali Sina University, Hamedan, 65178-38695, Iran*

*Corresponding Author, Tel.: +988138292505; Fax: +98 813 8257400

E-Mail: a.fattah@basu.ac.ir

*Received: 20 October 2018 / Accepted with minor revision: 11 January 2019 / Published online: 31 January 2019*

**Abstract**- In this research, plasma electrolytic oxidation (PEO) coating on AZ31B magnesium alloy having various concentrations has been studied in order to amend the surface corrosion resistance. To do this, phosphate electrolyte with different concentrations of 4, 8 and 10 g/l is investigated. Electrochemical impedance spectroscopy and potentiodynamic polarization tests on an uncoated base alloy and a coated one are studied in a body simulant physiological solution (Ringer's solution). Surface morphology and microstructural surveys were done by X-ray diffraction (XRD) pattern and scanning electron microscopy (SEM). The obtained results of this study displayed that rising the sodium phosphate concentration led to an increase in coating thickness and decreases its porosity. The highest corrosion resistance arose from the lowest corrosion current density ($0.45\times10^{-6}$ A/cm$^2$) of the formed coating in electrolyte containing 10 g/l sodium phosphate.

**Keywords**- Plasma electrolytic oxidation, AZ31B magnesium alloy, Electrochemical Impedance Spectroscopy, Potentiodynamic polarization

## 1. INTRODUCTION

Having a density of 74.1 grams per cubic meter, Magnesium is one of the lightest metals [1]. The high strength to weight, having good casting ability under controlled conditions, machining ability and impact properties are the most important privileges having developed its utility in diverse industries like electronics, aerospace and transportation [2,3]. Having the same mechanical properties as bone, Magnesium is being utilized in many medical applications [4]. The stress in the bone and implantation interface is declined as a result of Yang's modulus and density of magnesium and its alloys that augments bone growth and implantation stability [5]. However, with an electrochemical potential of -2.38 V than the hydrogen electrode, magnesium seems to be the earliest and oldest metal among metals and its alloys possess a poor corrosion resistance [6]. As magnesium alloys are susceptible of galvanic corrosion, this defect restricts the utility of non-shielded magnesium alloys in the corrosive environment. Magnesium and its alloys low corrosion resistance causes a decrement in mechanical stability and make an undesirable appearance, so carrying on surface process for these alloys looks vital [7]. AZ31B alloy is one of the widely used magnesium-aluminum-zinc triple alloys that is being utilized in aircraft bodies, mobile parts and biodegradable implants. As a single-phase alloy, AZ31B has about 3 percent aluminum and about 1 percent zinc in addition to a small amount of manganese, which is a solid solution in a magnesium crystal network [8]. Having a low corrosion resistance, surface treatments are necessary for this alloy. Diverse coating procedures such as plasma spraying methods [9], sol gel [10], physical vapor deposition [11], PEO [12] that can be mentioned, have been studied so far in order to protect magnesium and its alloys from corrosion. Among the mentioned methods above, the PEO process is a new surface procedure, being utilized in order to protect magnesium and its alloys from corrosion. Although an ordinary anodizing is beginning of this process, it ends with ignition. The ionic property alters the oxide layer into a thick ceramic coating having good properties, like high hardness, besides good corrosion and abrasion properties and strong cohesion with the substrate [13]. Being capable of coating huge and complex shapes, the simplicity of the equipment and using alkaline electrolytes, this process is not hazardous for the environment and the creatures and no harmful emissions are spread in the environment through the process. This process is based on anodic oxidation of light metals and their alloys in alkaline electrolytic solutions [14].

In the present study, we examined effect of sodium phosphate concentration on corrosion behavior of the coatings produced by PEO on AZ31B Mg alloy. The PEO coatings produced with different concentrations of 4, 8 and 10 g/l of sodium phosphate electrolyte. The microstructure and micro pores in the different coatings studied. Also the corrosion behavior of the coatings in Ringer's solution investigated.

## 2. EXPERIMENTAL PROCEDURE

As shown in Table 1, AZ31B magnesium alloy sheet with the provided chemical composition has been utilized in the coating process. Carrying on the coating process, the samples were cut by wire cutting machine as rectangular cubes having dimensions of 20×15×20 mm. Before starting the coating process, all samples were sanded using emeries having SiC particles with sizes of 220, 400, 600, 800 and 1000, respectively, and then washed applying distilled water and then dried by cold air. In this process, the stainless steel container having electrolyte plays the role of the cathode whereas the nugget is considered as the anode. The used electrolyte to do the coating process just contains sodium phosphate. As can be seen in Table 2, distinct sodium phosphate concentrations ($Na_3PO_4.12H_2O$) are indicated. The power supply of 700/7 PRC (IPS) PM model was utilized in order to perform the coating process. This power supply which has been used in this study is capable of operating in direct, simple, direct pulse and intermittent modes. Moreover, this apparatus is capable of utilizing in either constant current or constant voltage mode. Constant voltage (420 volts) and simple direct mode were utilized in this research.

Potentiodynamic polarization tests and electrochemical impedance spectroscopy (EIS) on an uncoated AZ31B magnesium alloy and a coated one were carried out in the body simulated physiological solution of Ringer. The μautolab potentiostat apparatus was used in a three-electrode method in electrochemical tests as follows: silver wire in silver/silver chloride saturation solution (Ag/AgCl) as the reference electrode and the platinum rod as an auxiliary electrode and the test samples were utilized as a working electrode. The specimens were initially put in a corrosion solution for 30 min in order to reach the steady state under open-circuit potential conditions. The EIS was carried out at a frequency range of 100 kHz to 10 mHz with a wavelength amplitude of ±10 mV. SEM (JEOL JSM-840 A) device was utilized to consider the coatings microstructure and thickness. Furthermore, Image J was used to measure the coatings thickness. In this study, the XRD pattern of Grazing method using a Philips PW1730 diffuser at 20 to 80 degree diffraction angle was utilized for specifying the present phases of the samples. The Xpert High Score software was used in order to identify the obtained peaks according to the existing standards of the desired phases.

**Table 1.** Chemical composition of AZ31B magnesium alloy

| **Element** | Ca | Zn | Si | Ni | Fe | Mn | Al | Mg |
|---|---|---|---|---|---|---|---|---|
| **Wt%** | 0.006 | 0.96 | 0.01 | 0.01 | 0.006 | 0.39 | 2.65 | Surplus |

**Table 2.** The chemical composition of used electrolytes in the PEO process

| **Sample** | **A** | **B** | **C** |
|---|---|---|---|
| **Sodium phosphate (g/l)** | 4 | 8 | 10 |

## 3. RESULTS AND DISCUSSION

### 3.1. Surface microstructure

Fig. 1 displays SEM images of PEO coatings. Surface of coatings have a porous structure with dimensions of several hundred nanometers to about a few micrometers on account of sparking during coating operations. Porosities are created while the oxide layer melting and results in releasing oxygen during the coating process and gas bubbles are thrown out of the micro-arc discharge channels [15]. The characteristics of sparks like size, intensity and lifetime influence formation of porous structure [16]. Fig. 1 (a) to (c) indicate that microstructure is the function of concentration and electrical conductivity of the solution in the coating process. Thus, the porosity percentage in the coating diminishes while increasing electrolyte concentration.

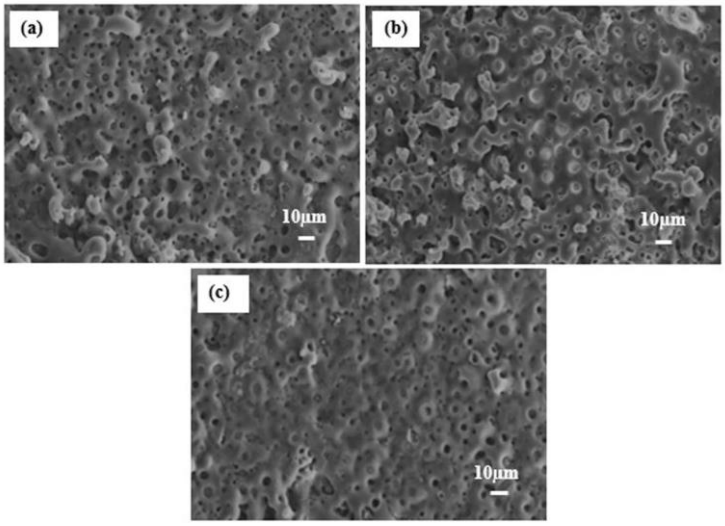


**Fig. 1.** SEM surfaces of PEO process (a) sample A; (b) sample B; and (c) sample C at magnification of 500 times

### 3.2. Coatings cross-sections

Fig. 2 illustrates the coatings cross-sections in various electrolytes. Coatings created by PEO include two layers. An inner layer being in contact with the substrate that has been

described as dense, compact, and functional and an outer layer having porous and crispy nature [17]. Cross section images show that the formation rate of oxide layer rises while increasing sodium phosphate concentration and this results in having a thicker coating.

Fig. 3 illustrates the column graph related to porosity percentage and coating thickness amounts in different baths. As can be seen in Fig. 3, increasing the sodium phosphate concentration during the coating process led to a decrease in the porosity percentage. The results also indicate that increasing salt concentration of sodium phosphate from 4 to 10 grams per liter led the coating thickness to rise from 11.5 to 28.7 μm. Intense spark discharge causes porosity in the coating of 10 g/l sodium phosphate, as displayed in the image of the coating thickness.

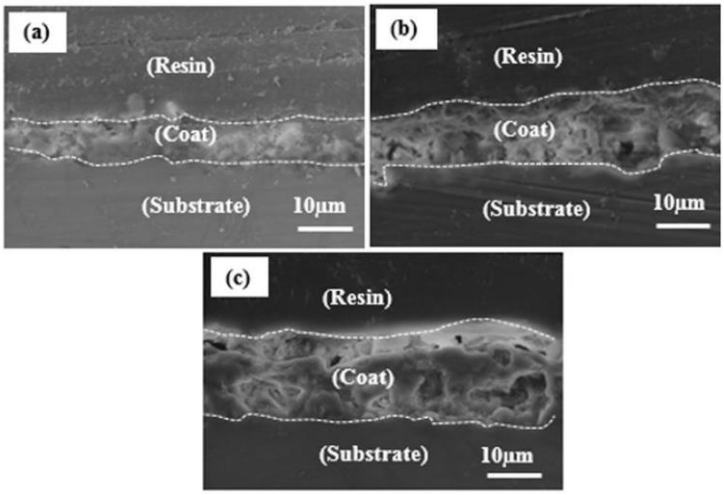


**Fig. 2.** The cross section of the obtained coatings using PEO process (a) sample A; (b) sample B and (c) sample C

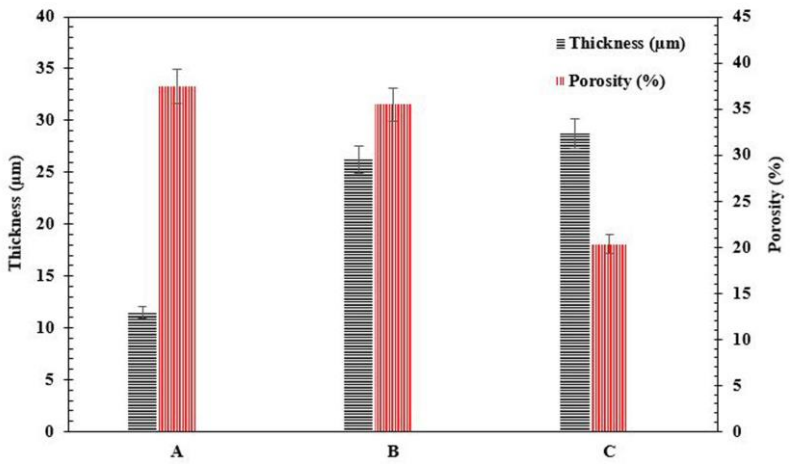


**Fig. 3.** Thickness and porosity percentage of created coatings at different concentrations of sodium phosphate

### 3.3. XRD pattern analysis

The normal XRD analysis includes peaks of high intensity from the substrate and weak peaks from the coating layer. A Grazing test is utilized in order to cope with this problem as well as achieving the applied coating chemical composition. Having an angle of one degree which remains constant within the analysis, the X-ray hits a specimen in this method and just the device detector performs the scanning operation. Considering low angle of beam collision to the sample, the penetration depth of the radiation will diminish in the sample and helpful information about the coating will be provided. Fig. 4 illustrates the XRD pattern using Grazing method for a coated sample containing 10 g/l. The formed phases within the PEO procedure depend on the used electrolyte chemical composition. The XRD pattern using Grazing method after the coating process indicates formation of phases in the coating which the $Mg_2P_2O_7$ phase and $NaMg(PO_3)_2$ presence imply the reaction between the obtained anions from the phosphate salt and the cation from the substrate the dissolution.

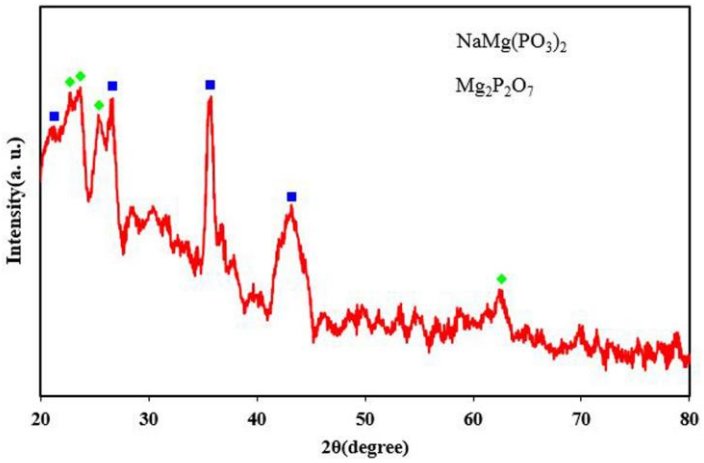


**Fig. 4.** XRD pattern by Grazing method for coating with 10 g/l phosphate

### 3.4. Corrosion behavior

*3.4.1. EIS test*

EIS test was carried out in order to achieve comprehensive data regarding the corrosion behavior of coatings created at different sodium phosphate concentrations in a Ringer solution. The Bode and Nyquist curves obtained from the EIS test for coated samples and substrate are illustrated in Fig. 5. Nyquist diagrams of the coated samples at sodium phosphate distinct concentrations have the same shapes and all of them consist of two half loops (Fig. 5a). The smaller half loop that is seen at high frequencies is related to the porous outer layer and the larger half loop is related to the compact inner layer being observed at low frequencies. Comparing the curves ring diameter in the Nyquist diagram, it is easily observed that specimen C has the largest ring diameter and so possesses the highest corrosion resistance. As can be

seen in the Bode curve (Fig. 5b), the highest impedance amount (Z) is related to sample C at low frequencies. Thus, it is concluded that the best obtained corrosion behavior is for the produced coating at sodium phosphate concentration of 10 g/l (sample C).

The coated samples have two capacitive half- loops being utilized in order to process the impedance data from the equivalent electrical circuit of Fig. 6. In this equivalent circuit, $R_s$ stands for solution resistance between the surface of the coating and the reference electrode, $R_{inne}$ and $Q_{inner}$ are related to the corrosion resistance and internal compressed layer fixed phase element respectively and the $R_{outer}$ and $Q_{outer}$ are related to the corrosion resistance and external porous layer fixed phase element respectively. The obtained values of elements are shown in Table 3.

The acquired results from modeling the obtained data of the impedance spectrum by the equivalent circuit of Fig. 6 is illustrated in Table 3. The results indicate that the coatings resistance is much higher than the substrate. The corrosion resistance of AZ31B alloy augmented to 37 times more applying PEO coatings. The inner layer resistance value ($R_{inner}$) is obviously much larger than the outer layer resistance ($R_o$) for all of the coatings. This issue shows that the inner dense layer plays a more important role in protecting coatings from corrosion. Moreover, the internal and external layers resistance augments by rising the sodium phosphate concentration from 4 to 10 grams per liter. Therefore, the sample containing 10 g/l sodium phosphate has the highest resistance of internal layer (630 kΩ/cm$^2$) and external layer resistance (30.50 kΩ/cm$^2$), and thus the best corrosion behavior.

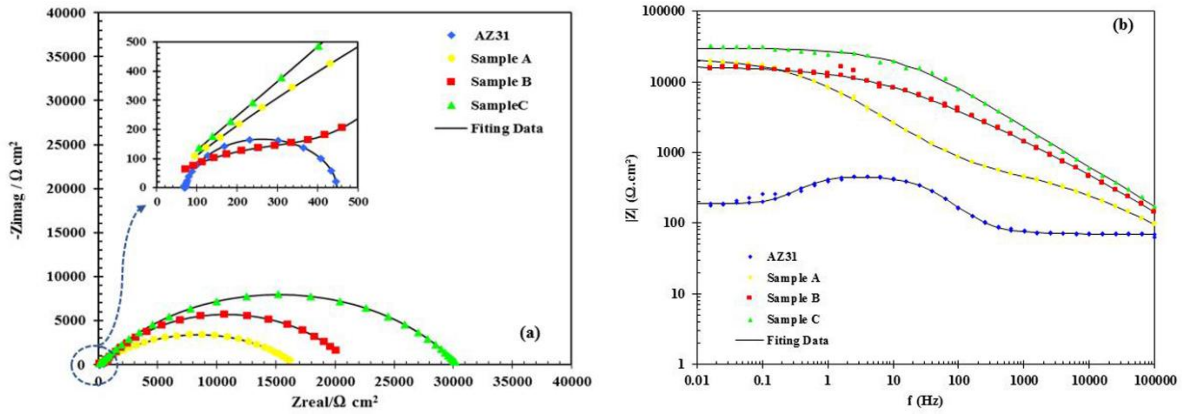


**Fig. 5.** (a) Nyquist and (b) Bode plots for AZ31B alloy and coated samples at sodium phosphate different concentrations.

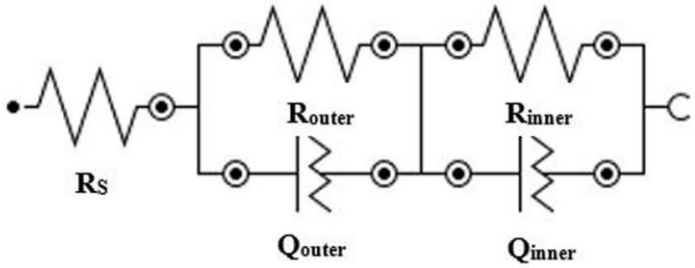


**Fig. 6.** Equivalent electrical circuit to model coatings corrosion behavior

**Table 3.** Obtained impedance parameters from equivalent circuit

| Sample | $R_{inner}$ (kΩ cm$^2$) | $R_{outer}$ (kΩ cm$^2$) |
|---|---|---|
| AZ31B | --- | 0.42 |
| A | 453 | 15.75 |
| B | 544 | 20.41 |
| C | 630 | 30.50 |

*3.4.2. Potentiodynamic polarization test*

Fig. 7 indicates the potentiodynamic polarization diagram for uncoated and coated samples in body simulated solution. The tests were performed with a scanning rate of 1 mV/s, ranging from -250 mV to +250 mV, toward the open circuit potential. The curve has two cathodic and anodic branches indicating the corrosion potential variations according to current density. Corrosion current density has been obtained using the Tafel extraction method, which make us capable of measuring polarization resistance accurately. Applying ceramic coatings on the AZ31B alloy, the potentiodynamic polarization curves of all coatings toward the substrate are transferred to a more negative potential and lower corrosion density. This shows that, the thermodynamic tendency to create corrosion phenomena has increased, whereas the kinetics of corrosion is reduced applying a ceramic coating. The polarization resistance can be calculated using the Stern-Geary equation [18]:

$$R_p = \frac{\beta_a \beta_c}{2.3(\beta_a + \beta_c) i_{corr}} \quad (1)$$

In this equation, $\beta_a$ and $\beta_c$ are the slope of anode and cathode branches respectively, $i_{corr}$ is the corrosion current density and $R_p$ is the polarization resistance. Being one of the most significant defects in PEO coatings, porosities play a major role in different properties of coating especially in corrosion resistance, because corrosive liquid can penetrate inside the coating through these porosities and having destructed the coating, they reach the substrate at last. Equation 2 clarifies the relation between the porosity percentage of the coating and the electrochemical parameters acquired from the potentiodynamic polarization curves in which P is the porosity percentage of the coating, $R_{ps}$ and $R_p$, are the corrosion resistance of the substrate and the coating respectively, $\beta_a$ is the substrate anodic branch slope, and $\Delta E_{corr}$ shows the potential corrosion difference between the substrate and the coating [19,20].

$$p = \left(\frac{Rps}{Rp}\right) \times 10^{-\left(\frac{\Delta Ecorr}{\beta a}\right)} \times 100 \quad (2)$$

The electrochemical data extracted from Fig. 7 including corrosion potential ($E_{corr}$), corrosion current density ($i_{corr}$), slope of anodic and cathodic branches ($\beta_a$ and $\beta_c$), polarization resistance ($R_p$), and porosity percentage are listed in Table 4. A good accordance exists between the porosity percentage obtained from SEM images with the porosity percentage gained from equation (2).

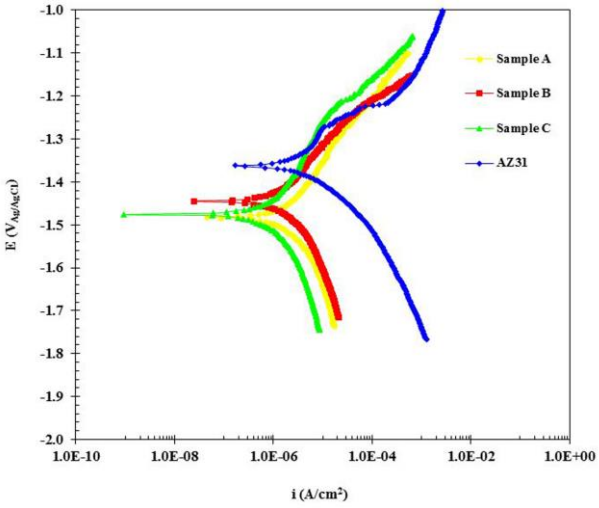


**Fig. 7.** Potentiodynamic polarization plots of the coatings in the body simulated solution

**Table 4.** Polarization parameters acquired from potentiodynamic polarization curves

| Sample | $b_a$ (mV/dec) | $b_c$ (mV/dec) | $i_{corr}$ (A cm$^{-2}$) | $E_{corr}$ (mV) | $R_p$ (kΩ cm$^2$) | P(%) |
|---|---|---|---|---|---|---|
| AZ31B | 41.37 | 61.21 | $8.23\times10^{-6}\pm 2\times10^{-7}$ | -1.36 | 12.95 | --- |
| A | 26.63 | 27.61 | $1.56\times10^{-6}\pm 1\times10^{-7}$ | -1.48 | 36.25 | 34 |
| B | 20.05 | 22.46 | $1.35\times10^{-6}\pm 2\times10^{-8}$ | -1.44 | 40.04 | 31 |
| C | 23.76 | 21.21 | $0.45\times10^{-6}\pm 1\times10^{-8}$ | -1.47 | 84.81 | 14 |

All three coated samples have higher corrosion resistance comparing with the uncoated sample. This issue displays that the corrosion resistance of the substrate is significantly increased by the PEO process. Comparing the corrosion resistance of the coatings and the reported porosity in Table 4, a correlation between these two parameters is discovered. Rising sodium phosphate concentration, there will be a decline in the porosity percentage and an increase in polarization resistance. The sample C has the lowest porosity percentage (14%) and also the lowest corrosion current density ($0.45\times10^{-6}$ A/cm$^2$), and therefore the highest polarization resistance (84.81 kΩ/cm$^2$).

## 4. CONCLUSION

In this investigation, the coating corrosion behavior and microstructure on AZ31B magnesium alloy were studied using PEO process. EIS measurements and potentiodynamic polarization indicated the PEO process amended the corrosion behavior of AZ31B magnesium alloy effectively. Increasing the concentration of sodium phosphate, the corrosion current density of the coated samples was diminished. Thus, the coating obtained from the bath having 10 g/l sodium phosphate had the lowest corrosion current density ($0.45\times10^{-4}$ A/cm$^2$). The SEM images obtained from PEO indicated that increasing sodium phosphate concentration, porosity percent decreased from 37.4% to 20.3%. Also, the coated samples cross sections images displayed that, increasing phosphate concentration from 4 to 10 g/l led the sample thickness to range from 11.5 μm to 28.71 μm. Electrolyte containing sodium phosphate produced $Mg_2P_2O_7$ and $NaMg(PO_3)_2$ phases as a result of the reaction between the anion and the cation inside the electrolyte. This fact is shown using the obtained result from the XRD pattern by Grazing method.

## REFERENCES

[1] J. Ma, M. Thompson, N. Zhao, and D. Zhu, J. Orthopaedic Translation 2 (2014)118.
[2] A. Fattah-alhosseini, and M. Sabaghi Joni, J. Mater. Eng. Perform. 24 (2015) 3444.
[3] A. Fattah-alhosseini, and M. Sabaghi Joni, J. Alloy. Compd. 646 (2015) 685.
[4] S. Agarwal, J. Curtin, B. Duffy, and S. Jaiswal, Mater. Sci. Eng. C 68 (2016) 948.
[5] S. Narayanan, S. Park, and M. Lee, Prog. Mater. Sci. 60 (2014) 1.
[6] H. Dong, Surface engineering of light alloys: Aluminium, magnesium and titanium alloys (2010).
[7] A. Fattah-alhosseini, and M. Sabaghi Joni, J. Magnesium Alloy. 2 (2014) 175.
[8] F. Witte, N. Hort, C. Vogt, S. Cohen, K. Kainer, R. Willumeit, and F. Feyerabend, Current opinion in solid state and materials Science 12 (2008) 63.
[9] X. Liu, P. Chu, and C. Ding, Mater. Sci. Eng. R 47 (2004) 49.
[10] Y. Harada, and S. Kumai, Surface and Coatings Technol. 228 (2013) 59.

[11] G. Kaliaraj, M. Bavanilathamuthiah, K. Kirubaharan, D. Ramachandran, and K. Viswanathan, Surface and Coatings Technol. 307 (2016) 227.
[12] H. Riyad, Electronic Theses and Dissertations (2015) 6.
[13] M. Vakili-Azghandi, A. Fattah-alhosseini, and M.K. Keshavarz, J. Mater. Eng. Perform. 25 (2016) 5302.
[14] Q. Li, G. Liang, and Q. Wang, Modern Surface Eng. Treatments (2013) 75.
[15] A. Fattah-alhosseini, M. Vakili-Azghandi, and M.K. Keshavarz, Acta Metallurgica Sinica (English Letters) 29 (2016) 274.
[16] H. Tang, and Y. Gao, J. Alloy. Comp. 688 (2016) 699.
[17] O. Galvis, D. Quintero, J. Castaño, H. Liu, G. Thompson, P. Skeldon, and F. Echeverría, Surface Coat Technol. 269 (2015) 238.
[18] M. Stern, and A. L. Geary, Electrochem. Soc. 104 (1957) 56.
[19] M. Shokouhfar, and S. R. Allahkaram, Surface and Coatings Technol. 309 (2017) 767.
[20] A. M. Kumar, S. H. Kwon, H. C. Jung, and K. S. Shin, Mater. Chem. Phys. 149-150 (2015) 480.